Airborne spectral measurements of surface–atmosphere anisotropy for several surfaces and ecosystems over southern Africa

Charles K. Gatebe,[1,2] Michael D. King,[2] Steve Platnick,[2,3] G. Thomas Arnold,[2,4] Eric F. Vermote,[2,5] and Beat Schmid[6]

Received 29 March 2002; revised 26 June 2002; accepted 5 August 2002; published 25 March 2003.

[1] The Cloud Absorption Radiometer (CAR) was flown aboard the University of Washington Convair CV-580 research aircraft during the Southern Africa Regional Science Initiative 2000 (SAFARI 2000) dry season campaign and obtained measurements of bidirectional reflectance distribution function (BRDF) for a variety of natural surfaces and ecosystems in southern Africa. To measure the BRDF of the surface–atmosphere system, the University of Washington CV-580 banked at a roll angle of ~20° and flew circles about 3 km in diameter above the surface, taking approximately 2 min. Multiple circular orbits were acquired over selected surfaces so that average BRDFs could be acquired, smoothing out small-scale surface and atmospheric inhomogeneities. In this paper, we present results of BRDFs taken over two Earth Observing System (EOS) validation sites: Skukuza tower, South Africa (25.0°S, 31.5°E) and Mongu tower, Zambia (15.4°S, 23.3°E). Additional sites are discussed and include the Maun tower, Botswana (20.0°S, 23.6°E), Sua Pan, Botswana (20.6°S, 25.9°E), Etosha Pan, Namibia (19.0°S, 16.0°E), and marine stratocumulus clouds off the west coast of Namibia (20.5°S, 13.1°E). Results clearly show anisotropy in reflected solar radiation over the various surfaces types: savanna, salt pans, and cloud. The greatest anisotropy is observed over marine stratus clouds, which exhibit strong forward scattering as well as important water cloud scattering features such as the rainbow and glory. The BRDF over savanna is characterized by a distinct backscattering peak in the principal plane and shows directional and spectral variations. Over the pans, the BRDF is more enhanced in the backscattering plane than forward scattering plane and shows little directional variation. *INDEX TERMS:* 0315 Atmospheric Composition and Structure: Biosphere/atmosphere interactions; 1640 Global Change: Remote sensing; 1694 Global Change: Instruments and techniques; 9305 Information Related to Geographic Region: Africa; 3359 Meteorology and Atmospheric Dynamics: Radiative processes; 3360 Meteorology and Atmospheric Dynamics: Remote sensing; *KEYWORDS:* BRDF, SAFARI 2000, surface reflectance, airborne measurements, radiometer, multispectral

Citation: Gatebe, C. K., M. D. King, S. Platnick, G. T. Arnold, E. F. Vermote, and B. Schmid, Airborne spectral measurements of surface–atmosphere anisotropy for several surfaces and ecosystems over southern Africa, *J. Geophys. Res.*, *108*(D13), 8489, doi:10.1029/2002JD002397, 2003.

1. Introduction

[2] This paper discusses measurements of surface anisotropy for different surfaces and ecosystems in southern Africa obtained with NASA's Cloud Absorption Radiometer (CAR) aboard the University of Washington Convair CV-580 research aircraft. The measurements were obtained during the Southern Africa Regional Science Initiative 2000 (SAFARI 2000) dry season campaign between 10 August and 18 September 2000 [*Swap et al.*, 2002].

[3] The properties of anisotropically scattering surfaces in the reflection of solar incident light is described and specified by the bidirectional reflectance distribution function (BRDF). The BRDF provides a way of geometrically and quantitatively expressing the connection between radiance reflected from a location into a given direction and the incident irradiance at that location arriving from some other direction (including, in the case of retroreflection, the same direction) [*Nicodemus et al.*, 1977]. The BRDF is needed in remote sensing for the correction of view and illumination angle effects, for example, in image standardization and mosaicing [*Wu et al.*, 1995; *Li et al.*, 1996; *Strahler et al.*, 1996a]. It is also needed for deriving surface albedo [*Wanner et al.*, 1995; *Lewis*, 1995; *Strahler et al.*, 1996b;

[1]Goddard Earth Science and Technology Center, University of Maryland Baltimore County, Baltimore, Maryland, USA.
[2]Earth Sciences Directorate, National Aeronautics and Space Administration (NASA) Goddard Space Flight Center, Greenbelt, Maryland, USA.
[3]L3 Communications—EER Communications Systems, Inc., Chantilly, Virginia, USA.
[4]Department of Geography, University of Maryland, College Park, Maryland, USA.
[5]Bay Area Environmental Research Institute, Sonoma, California, USA.
[6]NASA Ames Research Center, Moffett Field, California, USA.

0148-0227/03/2002JD002397$09.00

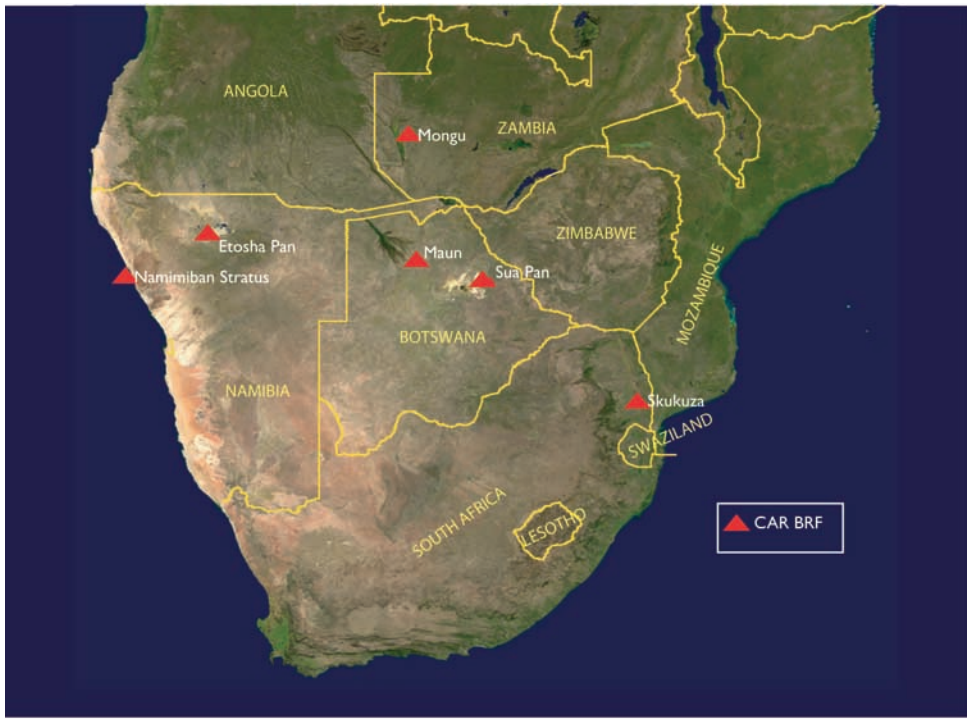

Figure 1. Locations of airborne measurements of BRDF obtained during the SAFARI 2000 field experiment from 12 August to 16 September 2000 using NASA s CAR. The background image on which the BRDF locations are mapped is a color composite of MODIS surface reflectance produced from atmospherically corrected 8-day MODIS reflectance data product.

Leroy et al., 1997]. Since albedo is an angular-weighted integration of reflection function over a hemisphere, the acquisition of radiometric measurements at different angles may improve its accuracy [e.g. Kimes et al., 1987]. Accurate albedo measurements are not only important for assessing the role of albedo in energy balance schemes [e.g. Kuusta et al., 1989] but are also important for accurate weather and climate modeling [e.g. Dickinson et al., 1990; Lean and Rowntree, 1997]. Some studies have shown that the BRDF can be used to improve land cover classification [e.g. Cihlar et al., 1994; Gutman, 1994; Moody and Strahler, 1994; Wu et al., 1995], for cloud detection [e.g. DiGirolamo and Davies, 1994; d'Entremont et al., 1996; Leroy et al., 1997], and for atmospheric correction [e.g. Kaufman, 1989]. This underpins the importance of BRDF measurements, a fact recognized more than three decades ago [e.g. Solomonson and Marlatt, 1968, 1971].

[4] The CAR [King et al., 1986] flying aboard the University of Washington aircraft has provided a convenient and efficient means of obtaining complete BRDFs for several surfaces types at a landscape level. Figure 1 shows the location of all sites for which CAR BRDF measurements were obtained throughout the SAFARI 2000 dry season campaign. In addition to these observations, CAR BRDF measurements have previously been obtained of a smoke layer from the Kuwait oil fires at 0.75 and 1.64 m [King, 1992], cerrado, dense forest, and smoke from forest fires in Brazil [e.g. Tsay et al., 1998], the Saudi Arabian desert, forested wetland (Great Dismal Swamp), and ocean water containing Sun glint over the Atlantic Ocean and the Persian Gulf [e.g. Bouillen et al., 2000], and four common arctic surfaces (snow-covered sea ice, melt-season ice, snow-covered tundra, and tundra shortly after snowmelt) [Arnold et al., 2002]. In this paper, we discuss BRDF measurements of various surfaces throughout southern Africa, including savanna, salt pans, and marine stratocumulus clouds off the coast of Namibia. More importantly, this paper examines the sensitivity of atmospheric correction to errors in aerosol optical depth and its angular dependence.

[5] The remainder of this paper is organized into four sections. Section 2, the theory, discusses the principal approach and formulation used to compute BRDF, while section 3 focuses on the instrument, calibration, BRDF measurement method, and atmospheric correction. Section 4 presents our results of the spectral BRDF and is thematically arranged to reflect similarities of the surfaces types: savanna, salt pans, and clouds. Section 5 concludes with a summary of the study.

2. Theory

[6] The bidirectional reflectance distribution function (BRDF) gives the reflectance of a target as a function of illumination geometry and viewing geometry, hence carries information about the anisotropy of the surface. It depends on wavelength and is determined by the structural and optical properties of the surface, such as shadow-casting, multiple scattering, mutual shadowing, transmission, reflection and absorption by surface element facet orienta-

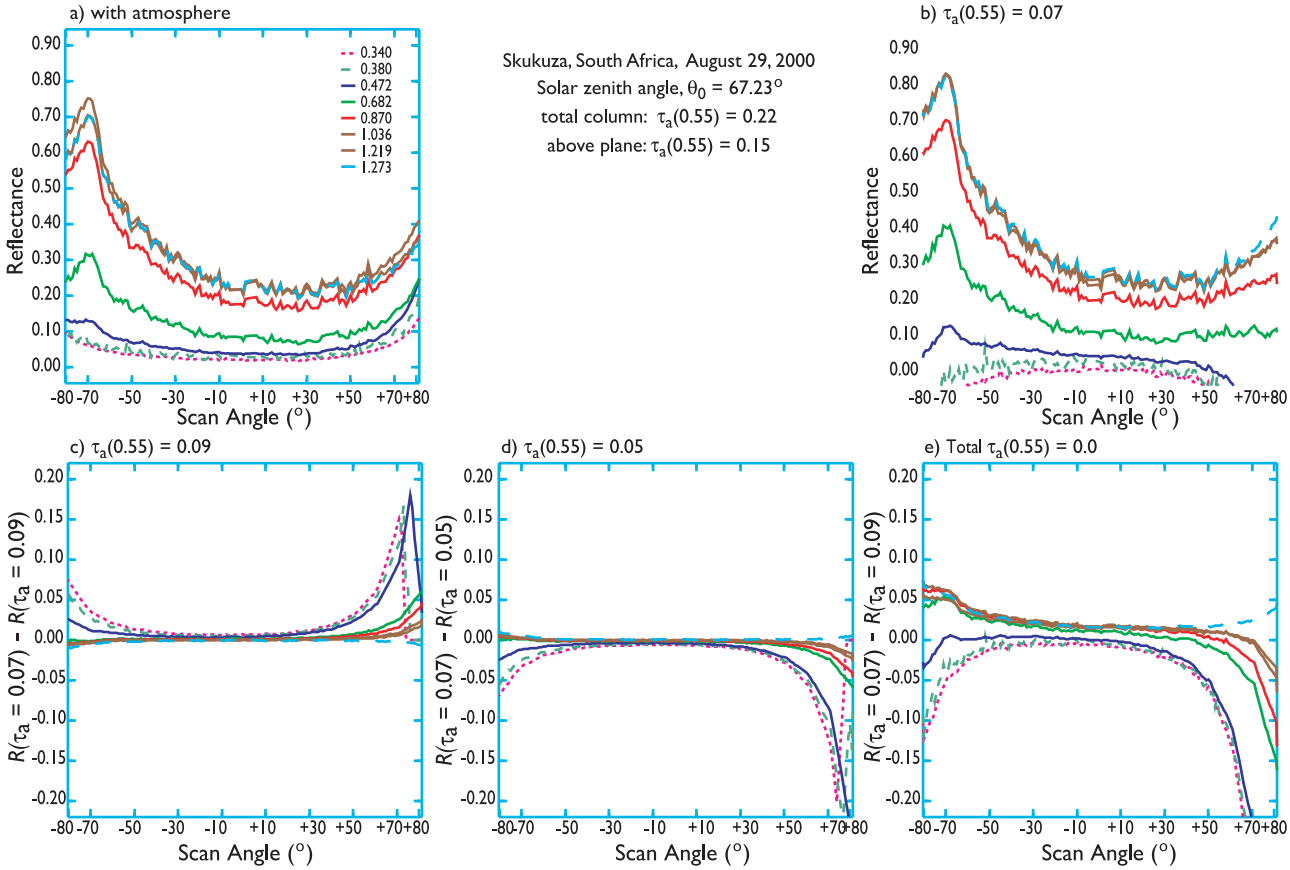

Figure 4. Angular distribution of bidirectional reflectance function in the principal plane (i.e., the vertical plane containing the Sun) for measurements taken over Skukuza, South Africa, (25.5°S, 31.5°E) to demonstrate the uncertainty associated with atmospheric correction. (a) No atmospheric correction has been applied. (b) Atmospheric correction has been applied for $\theta_0 = 67.8$, $\tau_a^{total}(0.550) = 0.22$, and O_3 = 300 m atm cm, where $\tau_a(0.550) = 0.07$ and H_2O = 0.94 g cm^{-2} below the plane. We have assumed a bimodal aerosol size distribution with complex index of refraction $n_r = 1.51 - 0.021i$. (c) Difference in reflectance between atmospheric correction below the plane for $\tau_a(\lambda) = 0.07$ and $\tau_a(\lambda) = 0.09$. (d) Same as (c) but difference in reflectance between $\tau_a(\lambda) = 0.07$ and $\tau_a(\lambda) = 0.05$. (e) Same as (b) but difference in reflectance between $\tau_a(\lambda) = 0.07$ and $\tau_a(\lambda) = 0.0$ for the total column.

angles for source and view directions, and hence, yield only average values over the angular intervals. The definition of R in (1) assumes a single direction for irradiance and reflectance over an area of a uniform and isotropic surface. This is the equation we have used to compute the BRDF discussed in this study.

[9] From the BRDF, we can derive the spectral albedo or the radiance reflected from the surface into all viewing directions and solid angles, by integrating the reflection function over solid angle. Hence, (1) becomes

$$r = \frac{1}{\pi} \int_0^{2\pi} \int_0^{\pi/2} R(\theta_0, \cos\theta \sin\theta \, d\theta \, d\phi \approx \frac{1}{\pi} \sum_{i=1}^{M} \sum_{j=1}^{N} I(\theta_0, \phi_j) \cos\theta_i \sin\theta_i \Delta\theta_i \Delta\phi_j \quad (2)$$

where (i,j) are indices for discretization of θ and ϕ over the hemisphere. In the present study we will not present albedo calculations, but will leave such comparisons with the spectral albedo from the Solar Spectral Flux Radiometer (SSFR) onboard the Convair CV-580 [King et al., 2003] and other related instrumentation during SAFARI 2000 to a future study.

3. Measurement Methods

3.1. Description of the Instrument

[10] In the past, we described the CAR [King et al., 1986], but the instrument has recently undergone several upgrades that include (1) adding and/or substituting optical channels to suit specific experimental objectives and (2) replacing the data system with a new data system with onboard signal digitization at 16 bit dynamic range and with improved signal-to-noise characteristics (see www.car.gsfc.nasa.gov for further details). Since these upgrades have not been described previously, we provide a short overview of the instrument in its present configuration.

[11] The CAR (Figure 2) is an airborne multiwavelength scanning radiometer that can perform several functions including (1) determining the single scattering albedo of

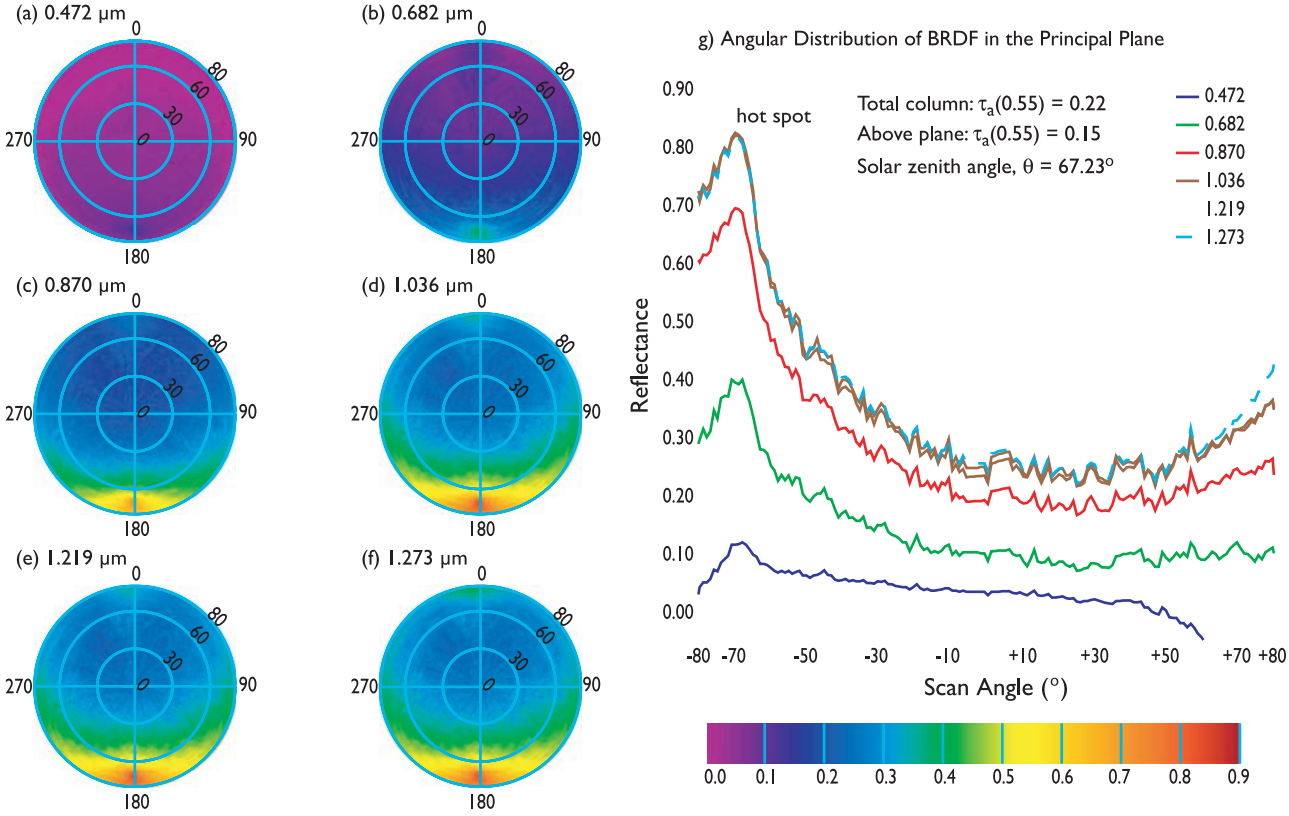

Figure 6. Spectral BRDF for selected CAR channels obtained over Skukuza, South Africa (25.0 S, 31.5 E) in late winter conditions (29 August 2000). In all polar plots, the viewing zenith angle is represented as the radial distance from the center and the azimuth as the length of arc on the respective zenith circle. The principal plane resides in the 180 azimuthal plane with the Sun located in the 180 azimuthal direction and is shown to the right of the polar plots. With this definition, the upper half circle represents forward scattering and the lower half circle backscattering. Atmospheric correction was applied using the following inputs: solar zenith angle = 67.23, total column $_a$( ) = 0.22 ($_a$( ) = 0.15 above the plane, = 0.550 m), and total column H$_2$O = 1.64 g cm^{-2} (H$_2$O = 0.73 g cm^{-2} above the plane). Other input parameters required for performing correction are as specified in Figure 4b.

note that the calibration ratios, postflight/preflight, vary between 1.048 (at = 0.340 m) and 1.292 (at = 1.556 m).

[17] For the spectral calibration, all spectral bands were scanned with a monochromator illuminated with a tungsten halogen lamp. The monochromator output was collimated and expanded to full input pupil of the CAR, and the beam was chopped to allow use of phase-sensitive signal detection. From these measurements, we determined the instrument system spectral response, central wavelength, and corresponding spectral band pass characteristics at each of the 14 spectral channels.

3.3. Measurements of BRDF

[18] To measure the BRDF of the surface atmosphere system, the aircraft flew at a roll angle of 20 flying in a circle about 3 km in diameter above the surface, taking roughly 2 3 min to complete an orbit (see Figure 3). The SAFARI 2000 measurements were generally obtained at an altitude of 600 m above the targeted surface and under clear sky conditions. Therefore, at a 1 FOV the pixel resolution is about 10 m at nadir and about 270 m at an 80 viewing angle from the CAR. Multiple circular orbits were acquired over a selected surface so that average BRDFs

average out small-scale surface and atmospheric inhomogeneities. With this configuration, the CAR collects between 76,400 and 114,600 directional measurements of radiance per channel per complete orbit.

[19] We believe using the CAR in this manner is the most mobile and efficient way of measuring a complete surface BRDF, but it is still necessary to correct for atmospheric scattering effects both above and below the aircraft in order to isolate the reflectance properties of the underlying surface in the absence of an atmosphere.

3.4. Atmospheric Correction

[20] We removed the effects of atmospheric absorption and scattering from our bidirectional reflectance functions using a new version of the second simulation of satellite signal in the solar spectrum (6S) model [Vermote et al., 1997]. The 6S code is a radiative transfer model based on the successive orders of scattering method. The spectral resolution of the model is 2.5 nm, and the aerosol layer is divided into 13 layers with a scale height of 2 km. The model assumes the atmosphere consists of fixed gases: O$_3$, H$_2$O, CO$_2$, CH$_4$, and N$_2$O. The concentration of O$_3$, CO$_2$, CH$_4$, and N$_2$O are assumed to be constant and

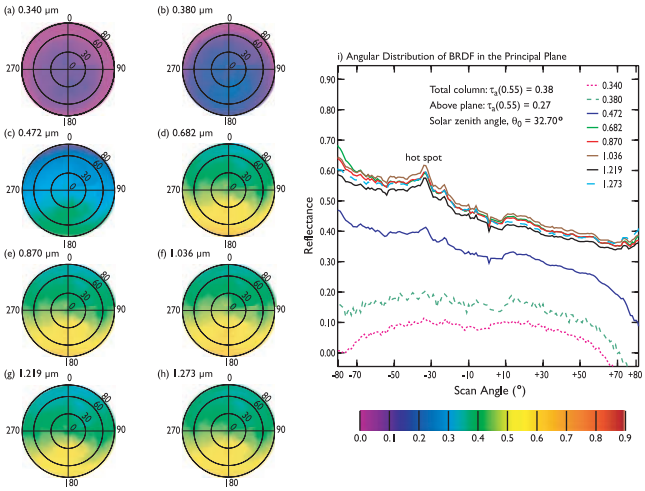

Figure 10. Spectral BRDF for selected CAR channels obtained over Etosha Pan (19.0°S, 16.0°E) in late winter conditions (16 September 2000). Atmospheric correction was applied using the following inputs: solar zenith angle $\theta_0 = 32.72°$, total column $\tau_a(\lambda) = 0.38$ ($\tau_a(\lambda) = 0.27$ above the plane, $\lambda = 0.550$ μm), and total column $H_2O = 1.13$ g cm^{-2} ($H_2O = 0.84$ g cm^{-2} above the plane). Other input parameters required for performing correction are as specified in Figure 4b.

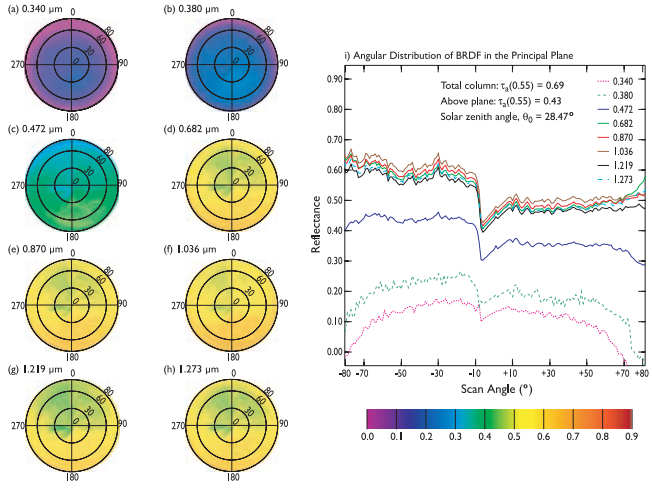

Figure 11. Spectral BRDF for selected CAR channels obtained over Sua Pan, Botswana (20.6°S, 25.9°E) in late winter conditions (3 September 2000). Atmospheric correction was applied using the following inputs: solar zenith angle $\theta_0 = 28.47°$, total column $\tau_a(\lambda) = 0.69$ ($\tau_a(\lambda) = 0.43$ above the plane, $\lambda = 0.550$ μm), and total column $H_2O = 1.04$ g cm^{-2} ($H_2O = 0.46$ g cm^{-2} above the plane). Other input parameters required for performing correction are as specified in Figure 4b.

gates create sufficient small-scale surface roughness that results in a dominant backscattering effect in the soil BRDF pattern. Soil spectral reflectance is controlled by other factors as well, including soil particle size, texture, organic matter, clay, iron content, soil moisture, and surface roughness. These properties determine not only the magnitude of the spectral reflectance but also the position and depth of spectral absorption features. Soil reflectance tends to increase steadily from about 0.2 in the visible and rarely exceeds 0.5 in the near infrared [*Nolin and Liang*, 2000]. Since the measured reflectance of the pan is in the range 0.2–0.6, we think that the salt pans are dominated by highly reflecting soil aggregates with very little organic matter.

[33] Figure 11 shows the BRDF of the Sua Pan (20.6°S, 25.9°E) and a transect through the principal plane for eight discrete wavelengths between 0.34 and 1.27 μm. The measurements reported here were obtained from 0949 to 1000 UTC for solar zenith angle $\theta_0 = 28.47°$. The BRDF pattern of Sua Pan is very similar to Etosha's enhanced reflectance in the backward scattering direction. The feature between $-10°$ and $+10°$ in the principal plane is a result of surface inhomogeneity that we were unable to avoid during our measurements.

4.3. BRDF of Marine Stratocumulus Offshore of Namibia

[34] The marine stratocumulus clouds off the western coast of southern Africa are layered clouds, associated with subtropical anticyclonic subsidence and cold water upwelling along the Benguela current [*Platnick et al.*, 2000]. These clouds are characterized by a well-defined cloud top height corresponding to a strong boundary layer inversion (Figure 5f). These clouds are impacted by both natural (sulfur from phytoplankton DMS production and decay processes) and anthropogenic sources (industrial and fire emission products) that can influence the clouds microphysical and optical properties, an effect that is not quantitatively well understood.

[35] Figure 12 shows the BRDF of marine stratus clouds and a transect through the principal plane of these clouds for

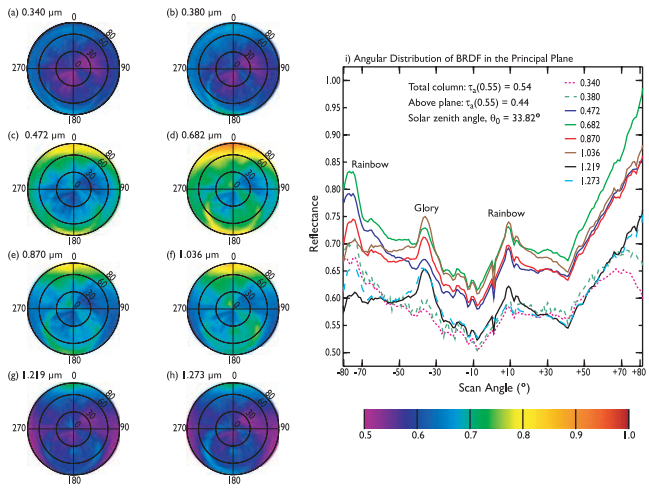

Figure 12. Spectral BRDF for selected CAR channels obtained over marine stratocumulus off the Skeleton coastline in Namibia (20.5°S, 13.1°E) in late winter conditions (13 September 2000). Atmospheric correction was applied using the following inputs: solar zenith angle $\theta_0 = 33.82°$, total column $\tau_a(\lambda) = 0.54$ ($\tau_a(\lambda) = 0.44$ above the plane, $\lambda = 0.550$ μm), and total column $H_2O = 0.86$ g cm^{-2} ($H_2O = 0.84$ g cm^{-2} above the plane). Other input parameters required for performing correction are as specified in Figure 4b.

eight discrete wavelengths between 0.34 and 1.27 μm. These measurements were obtained off the Namibian coast (20.5°S, 13.1°E) between 1228 and 1252 UTC for solar zenith angles $31° < \theta_0 < 36°$. Note the expanded scale of the color bar and reflectance axis, enabling more features and structure to be discerned. Visible in these BRDF observations for all spectral channels are pronounced circular brightness features, the rainbow and glory. These single scattering features are more distinct at 0.682 and 0.870 μm, and only barely visible at 0.340 μm, perhaps due more to lack of contrast perception. Looking at the angular distribution of BRDF in the principal plane (Figure 12i), we note that the primary rainbow has a peak at approximately −75° and +10°, corresponding to ∼42° from the antisolar direction characterized by the glory feature. The magnitude of reflectance in all spectral channels is between 0.5 and 0.9.

[36] Observations of the glory in both visible and near-infrared wavelengths have good potential as an approach to measuring cloud top droplet size through remote sensing. *Spinhirne and Nakajima* [1994] show a direct dependence of the glory-scattering angle on effective particle radius near the cloud top. The important and relevant characteristic is that the measurements would be unquestionably accurate and unambiguous. Our data along with coincident cloud microphysics and other measurements from SAFARI 2000 experiment (see Appendix A by P. V. Hobbs in the work of *Sinha et al.* [2003]) [*King et al.*, 2003] should enable us to conceive interesting analyses and applications for radiation and remote sensing problems.

5. Conclusions

[37] Between 12 August and 16 September 2000, the CAR onboard the University of Washington Convair CV-580 research aircraft obtained measurements of surface bidirectional reflectance of savanna, salt pans, and stratocumulus clouds throughout southern Africa as part of SAFARI 2000. To measure the BRDF of the surface–atmosphere system, the CV-580 had to bank at a comfortable roll angle of ∼20° and fly in a circle about 3 km in diameter above the surface for roughly 2 min. Multiple circular orbits were acquired over selected surfaces so that average BRDF smoothed out small-scale surface and atmospheric inhomogeneities. In this paper we presented results of BRDFs obtained over two EOS validation sites: Skukuza tower, South Africa (25.0°S, 31.5°E) and Mongu tower, Zambia (15.4°S, 23.3°E). Additional sites are discussed and include the Maun tower, Botswana (20.0°S, 23.5°E), Sua Pan, Botswana (20.6°S, 25.9°E), Etosha Pan, Namibia (19.0°S, 16.0°E) and marine stratus clouds off the west coast of Namibia (20.5°S, 13.1°E). The data presented in this paper have been corrected for atmospheric scattering and absorption using the 6S radiative transfer model.

[38] Results clearly show marked anisotropy in reflected solar radiation over various surfaces types, including savanna, salt pans and marine stratocumulus clouds. The greatest anisotropy in scattered radiation was observed over marine stratus clouds, and was characterized by strong forward scattering as well as water cloud scattering features in the backscattering direction, such as the rainbow and glory. The BRDF over savanna is characterized by a distinct peak in the antisolar direction whose magnitude and location in the principal plane depend on the solar zenith angle. The BRDF also shows distinct directional variations. Over salt pans, the BRDF is more enhanced in the backscattering plane than forward scattering plane and shows little directional variation. The pans show optical characteristics that are suggestive of highly reflecting soil aggregates with very little organic matter.

[39] **Acknowledgments.** The authors are especially grateful to P. V. Hobbs and the University of Washington CV-580 staff members for great assistance in data collection. Thanks also to P. K. Shu and team for engineering support, J. Y. Li and J. C. Riédi for support in data processing and analysis, W. H. Humberson and K. A. Gammage for providing graphics support, R. T. Dominguez and A. B. Coffland for providing Figures 5d and 5e, and P. A. Hubanks for providing color scale for the graphics. This research was supported by funding provided by the MODIS Science Team, the EOS Project Science Office, and NASA's Radiation Science Program. Funding to NASA Ames was provided by NASA's Earth Observing System Interdisciplinary Science (EOS-IDS) Program, Radiation Sciences Program, and Total Ozone Mapping Spectrometer (TOMS) Program (program codes 291-01-91-45, 622-44-75-10, and 621-14-01-00, respectively). The first author is grateful to the University of Nairobi, Kenya for granting a leave of absence. This research was conducted as part of the Southern African Regional Science Initiative (SAFARI 2000).

References

Arnold, G. T., M. D. King, S. C. Tsay, J. Y. Li, and P. F. Soulen, Airborne spectral measurements of surface–atmosphere anisotropy for Arctic sea ice and tundra, *Int. J. Remote Sens.*, *23*, 3763–3781, 2002.

Chandrasekhar, S., *Radiative Transfer*, 393 pp., Dover, Mineola, N. Y., 1960.

Chen, J. M., X. Li, T. Nilson, and A. Strahler, Recent advances in geometrical optical modeling and its applications, *Remote Sens. Rev.*, *18*, 227–262, 2000.

Cihlar, J., D. Manak, and N. Voisin, AVHRR bidirectional reflectance effects and compositing, *Remote Sens. Environ.*, *48*, 77–88, 1994.

d'Entremont, R. P., C. B. Schaaf, and A. H. Strahler, Cloud detection and land surface albedos using visible and near-infrared bidirectional reflectance distribution models, *Proc. 8th Conf. Satell. Meteorol.*, 334–338, 1996.

Dickinson, R. E., B. Pinty, and M. M. Verstraete, Relating surface albedos in GCMs to remotely sensed data, *Agric. For. Meteorol.*, *32*, 109–131, 1990.

DiGirolamo, L., and R. Davies, A band-difference angular signature technique for cirrus cloud detection, *IEEE Trans. Geosci. Remote Sens.*, *32*, 890–896, 1994.

Dubovik, O., and M. D. King, A flexible inversion algorithm for retrieval of aerosol optical properties from Sun and sky radiance measurements, *J. Geophys. Res.*, *105*, 20,673–20,696, 2000.

Dubovik, O., A. Smirnov, B. N. Holben, M. D. King, Y. J. Kaufman, T. F. Eck, and I. Slutsker, Accuracy assessment of aerosol optical properties retrieved from Aerosol Robotic Network (AERONET) Sun and sky radiance measurements, *J. Geophys. Res.*, *105*, 9791–9806, 2000.

Dubovik, O., B. N. Holben, T. F. Eck, A. Smirnov, Y. J. Kaufman, M. D. King, D. Tanré, and I. Slutsker, Variability of absorption and optical properties of key aerosol types observed in worldwide locations, *J. Atmos. Sci.*, *59*, 590–608, 2002.

Gatebe, C. K., M. D. King, S. C. Tsay, Q. Ji, G. T. Arnold, and J. Y. Li, Sensitivity of off-nadir zenith angles to correlation between visible and near-infrared reflectance for use in remote sensing of aerosol over land, *IEEE Trans. Geosci. Remote Sens.*, *39*, 805–819, 2001.

Gutman, G., Normalization of multi-annual global AVHRR reflectance data over land surfaces to common Sun-target-sensor geometry, *Adv. Space Res.*, *14*, 121–124, 1994.

Kaufman, Y. J., The atmospheric effect on remote sensing and its correction, in *Theory and Applications of Optical Remote Sensing*, pp. 336–428, John Wiley, New York, 1989.

Kaufman, Y. J., A. E. Wald, L. A. Remer, B. C. Gao, R. R. Li, and L. Flynn, The MODIS 2.1 μm channel—Correlation with visible reflectance for use in remote sensing of aerosol, *IEEE Trans. Geosci. Remote Sens.*, *35*, 1286–1298, 1997.

Kimes, D. S., P. J. Sellers, and D. J. Diner, Extraction of spectral hemispherical reflectance (albedo) of surface from nadir and directional reflectance data, *Int. J. Remote Sens.*, *8*, 1727–1746, 1987.

King, M. D., A method for determining the single scattering albedo of clouds through observation of the internal scattered radiation field, *J. Atmos. Sci.*, *38*, 2031–2044, 1981.

King, M. D., Directional and spectral reflectance of the Kuwait oil-fire smoke, *J. Geophys. Res.*, *97*, 14,545–14,549, 1992.
King, M. D., M. G. Strange, P. Leone, and L. R. Blaine, Multiwavelength scanning radiometer for airborne measurements of scattered radiation within clouds, *J. Atmos. Oceanic Technol.*, *3*, 513–522, 1986.
King, M. D., L. F. Radke, and P. V. Hobbs, Determination of the spectral absorption of solar radiation by marine stratocumulus clouds from airborne measurements within clouds, *J. Atmos. Sci.*, *47*, 894–907, 1990.
King, M. D., Y. J. Kaufman, D. Tanré, and T. Nakajima, Remote sensing of aerosols from space: Past, present, and future, *Bull. Am. Meteorol. Soc.*, *80*, 2229–2259, 1999.
King, M. D., S. Platnick, C. C. Moeller, H. E. Revercomb, and D. A. Chu, Remote sensing of smoke, land, and clouds from the NASA ER-2 during SAFARI-2000, *J. Geophys. Res.*, *108*, doi:10.1029/2002JD003207, in press, 2003.
Kustas, W. P., R. D. Jackson, and G. Asrar, Estimating surface energy-balance components from remotely sensed data, in *Theory and Applications of Optical Remote Sensing*, pp. 604–627, John Wiley, New York, 1989.
Lean, J., and P. R. Rowntree, Understanding the sensitivity of a GCM simulation of Amazonian deforestation to the specification of vegetation and soil characteristics, *J. Clim.*, *10*, 1216–1235, 1997.
Leroy, M., J. L. Deuzé, F. M. Bréon, O. Hautecoeur, M. Herman, J. C. Buriez, D. Tanré, S. Bouffiè, P. Chazette, and J. L. Roujean, Retrieval of atmospheric properties and surface bidirectional reflectances over land from POLDER/ADEOS, *J. Geophys. Res.*, *102*, 17,023–17,037, 1997.
Lewis, P., The utility of kernel-driven BRDF models in global BRDF and albedo studies, *Proc. Int. Geosci. Remote Sens. Symp.*, *95*, 1186–1187, 1995.
Lewis, P., M. I. Disney, M. J. Barnsley, and J. P. Muller, Deriving albedo maps for HAPEX-Sahel from ASAS data using kernel-driven BRDF models, *Hydrol. Earth Syst. Sci.*, *3*, 1–13, 1999.
Li, X., and A. H. Strahler, Geometric-optical bidirectional reflectance modeling of the discrete crown vegetation canopy: Effect of crown shape and mutual shadowing, *IEEE Trans. Geosci. Remote Sens.*, *30*, 276–292, 1992.
Li, Z., J. Cihlar, X. Zheng, L. Moreau, and H. Ly, The bidirectional effects of AVHRR measurements over boreal regions, *IEEE Trans. Geosci. Remote Sens.*, *34*, 1308–1322, 1996.
Moody, A., and A. H. Strahler, Characteristics of composited AVHRR data and problems in their classification, *Int. J. Remote Sens.*, *15*, 3473–3491, 1994.
Morisette, J. T., J. L. Privette, C. O. Justice, D. Olson, J. Dwyer, P. Davis, D. Starr, and D. Wickland, The EOS land validation core sites: Background information and current status, *Earth Observer*, *11*, 21–25, Nov/Dec 1999.
Nicodemus, F. E., J. C. Richmond, J. J. Hsia, I. W. Ginsberg, and T. Limperis, Geometric considerations and nomenclature for reflectance, U.S.A. Department of Commerce/National Bureau of Standards, *NBS Monogr.*, *160*, 1–52, 1977.
Nolin, A. W., and S. Liang, Progress in bidirectional reflectance modeling and applications for surface particulate media: Snow and soils, *Remote Sens. Rev.*, *18*, 307–342, 2000.
Platnick, S., S. A. Ackerman, R. A. Frey, and M. D. King, Remote sensing of Namibian marine stratocumulus clouds, paper presented at the 28th International Symposium of Remote Sensing of Environment (ISRSE), Somerset West, South Africa, March 27–31, 2000.
Salomonson, V. V., and W. E. Marlatt, Anisotropic solar reflectance over white sand, snow and stratus clouds, *J. Appl. Meteorol.*, *7*, 475–483, 1968.
Salomonson, V. V., and W. E. Marlatt, Airborne measurements of reflected solar radiation, *Remote Sens. Environ.*, *2*, 1–8, 1971.
Schmid, B., et al., Coordinated airborne, spaceborne, and ground-based measurements of massive, thick aerosol layers during the dry season in Southern Africa, *J. Geophys. Res.*, *108*, doi:10.1029/2002JD002297, in press, 2003.
Scholes, R. J., and S. R. Archer, Tree–grass interactions in savannas, *Annu. Rev. Ecol. Syst.*, *28*, 517–544, 1997.
Sinha, P., P. V. Hobbs, R. J. Yokelson, I. Bertschi, D. R. Blake, I. J. Simpson, S. Gao, T. L. Kirchstetter, and T. Novakov, Emissions of trace gases and particles from savanna fires in southern Africa, *J. Geophys. Res.*, *108*, doi:10.1029/2002JD002325, in press, 2003.
Soulen, P. F., M. D. King, S. C. Tsay, G. T. Arnold, and J. Y. Li, Airborne spectral measurements of surface–atmosphere anisotropy during the SCAR-A, Kuwait oil fire, and TARFOX experiments, *J. Geophys. Res.*, *105*, 10,203–10,218, 2000.
Spinhirne, J. D., and T. Nakajima, Glory of clouds in the near-infrared, *Appl. Opt.*, *33*, 4652–4662, 1994.
Strahler, A. H., J. T. Townshend, D. Muchoney, J. Borak, M. Friedl, S. Gopal, A. Hyman, A. Moody, and E. Lambin, MODIS land cover and land cover change: Algorithm technical basis document, *NASA EOS MODIS Doc.*, version 4.1, 102 pp., 1996a.
Strahler, A. H., W. Wanner, C. B. Schaaf, X. Li, B. Hu, J. P. Muller, P. Lewis, and M. J. Barnsley, MODIS BRDF/albedo product: Algorithm theoretical basis document, *NASA EOS-MODIS Doc. Incl. Update*, version 4.0, 252 pp., 1996b.
Swap, R. J., et al., The southern African regional science initiative (SAFARI 2000): Dry-season field campaign: An overview, *S. Afr. J. Sci.*, *98*, 125–131, 2002.
Tsay, S. C., M. D. King, G. T. Arnold, and J. Y. Li, Airborne spectral measurements of surface anisotropy during SCAR-B, *J. Geophys. Res.*, *103*, 31,943–31,954, 1998.
Tucker, C. J., Red and photographic infrared linear combinations for monitoring vegetation, *Remote Sens. Environ.*, *8*, 127–150, 1979.
van de Hulst, H. C., *Multiple Light Scattering, Tables, Formulas, and Applications*, vol. 1, pp. 76–82, Academic, San Diego, Calif., 1980.
Vermote, E. F., D. Tanré, J. L. Deuzé, M. Herman, and J. J. Morcrette, Second simulation of the satellite signal in the solar spectrum, 6S: An overview, *IEEE Trans. Geosci. Remote Sens.*, *35*, 675–686, 1997.
Wanner, W., X. Li, and A. H. Strahler, On the derivation of kernels for kernel-driven models of bidirectional reflectance, *J. Geophys. Res.*, *100*, 21,077–21,089, 1995.
Wanner, W., A. H. Strahler, B. Hu, P. Lewis, J.-P. Muller, X. Li, C. L. B. Schaaf, and M. J. Barnsley, Global retrieval of bidirectional reflectance and albedo over land from EOS MODIS and MISR data: Theory and algorithm, *J. Geophys. Res.*, *102*, 17,143–17,161, 1997.
Wu, A., Z. Li, and J. Cihlar, Effects of land cover type, greenness, and Sun angle on bidirectional distribution of advanced very high resolution radiometer reflectances, *J. Geophys. Res.*, *100*, 9179–9192, 1995.

G. T. Arnold, L3 Communications—EER Communications Systems, Inc., 3750 Centerview Drive, Chantilly, VA 20151, USA. (arnold@climate.gsfc.nasa.gov)

C. K. Gatebe, Goddard Earth Sciences and Technology Center, University of Maryland Baltimore County, Baltimore, MD 21228-5398, USA. (gatebe@climate.gsfc.nasa.gov)

M. D. King, S. Platnick, and E. F. Vermote, Earth Sciences Directorate, National Aeronautical and Space Administration (NASA), Goddard Space Flight Center, Greenbelt, MD 20771, USA. (michael.d.king@nasa.gov; steven.e.platnick@nasa.gov; eric@kratmos.gsfc.nasa.gov)

B. Schmid, NASA Ames Research Center, Moffett Field, CA 94035-1000, USA. (bschmid@mail.arc.nasa.gov)